ETH
Eidgenössische Technische Hochschule Zürich
Swiss Federal Institute of Technology Zurich

Cancellation of phase noise induced by an optical fiber in a compact setup

Semester Project Report

Pedro Rosso Gómez

Friday 8th March, 2019

Supervisor: Chiara Decaroli

Prof. Jonathan P. Home - Trapped Ion Quantum Information Group
Institute for Quantum Electronics, ETH Zürich

Abstract

Experiments with trapped ions require lasers for the preparation and manipulation of the ion's quantum states. Due to the long running time of these experiments and the high sensitivity of the ions, the laser beam must be as coherent as possible. In this report, we present a compact technical setup with the purpose of eliminating the slow optical phase noise induced by the fiber which delivers the laser beam to the ions. The setup consists of an acousto-optic modulator (AOM), its acoustic signal generator, an electronic circuit which implements a feedback loop and a photodiode. The back reflection from the fiber is aligned into the photodiode, which produces an electric signal whose spectrum is dependent on the phase noise. This signal is used by the electronic circuit to modulate the signal produced by the acoustic generator such that the phase noise in the beam is canceled out by the AOM.

Contents

Chapter 1

Introduction

Since the birth of quantum mechanics several thought experiments have been proposed which involve the manipulation of quantum systems and many real experiments have been performed which confirm the theoretical predictions. The main challenge nowadays is the physical implementation of such systems; while there is a wide range of possibilities (quantum dots, superconducting circuits), we shall focus on the trapped ion platform [CZ95, Kie15]. The ions are captured in ion traps: devices which generate electromagnetic fields such that there is a region in which the ion is trapped [Mat16]. As soon as one is caught, it is possible to manipulate it using short, coherent laser pulses. Given that any noise in the laser beam signal may reduce the lifetime of the quantum system, it is necessary to make sure that any fluctuations in the laser frequency are properly suppressed [Fis13, Flu14, Sep12, Opp15]. The objective of this semester project is to reduce the phase noise caused by the optical fiber which delivers the laser beam to the ion trap.

1.1 The calcium ion and its quantum states

The singly charged $^{40}\mathrm{Ca}^+$ ion has several properties that make it appropriate for experiments which involve quantum system manipulation. It has only one electron in its valence shell and no nuclear spin. Both characteristics simplify the quantum states representation, given that there is no hyperfine structure and the electrons in the lower orbits have a small influence on the valence electron [Kie15]. With this information, it is possible to treat the ion's quantum states as a tensor product of the valence electron spin and its orbit:

$$|\phi\rangle = \sum_{l,m,m_s} c_{l,m,m_s} |l,m\rangle \otimes |m_s\rangle \equiv \sum_{l,m,m_s} c_{l,m,m_s} |l,m,m_s\rangle\,, \tag{1.1}$$

where the indexes l, m indicate the orbital and the index m_s indicate the valence electron's spin. Any state $|\phi\rangle$ can be represented as a normalized linear combination of the base states $|l,m,m_s\rangle$ [Gab18].

The energy levels of $^{40}\mathrm{Ca}^+$ is presented in figure 1.1. The dipole transition $S_{1/2}$ to $P_{1/2}$, which is driven with a laser at 397 nm, is used for Doppler cooling and fluorescence detection. It has a repumper at 866 nm recycling population decaying from the $P_{1/2}$ to the $D_{3/2}$ state [Kie15]. Of special interest is the $S_{1/2}$ to the $D_{5/2}$ quadrupole transition: it is forbidden by the selection rules [Hom17], which means that an ion in state $D_{5/2}$ has a reasonable long lifetime and does not spontaneously decay into the state $S_{1/2}$. By defining $|\uparrow\rangle \equiv D_{5/2}$ and $|\downarrow\rangle \equiv S_{1/2}$, the representation is constrained to a two dimensional subspace, and any state $|\psi\rangle$ is now of the form:

$$|\psi\rangle = \alpha\,|\uparrow\rangle + \beta\,|\downarrow\rangle\,, \tag{1.2}$$

$$\alpha, \beta \in \mathbb{C}, \qquad |\alpha|^2 + |\beta|^2 = 1, \tag{1.3}$$

where $|\alpha|^2$ and $|\beta|^2$ are the probabilities of finding the electron on state $|\uparrow\rangle$ and $|\downarrow\rangle$, respectively. The optical transition has an energy corresponding to light with 729 nm wavelength, which means that in

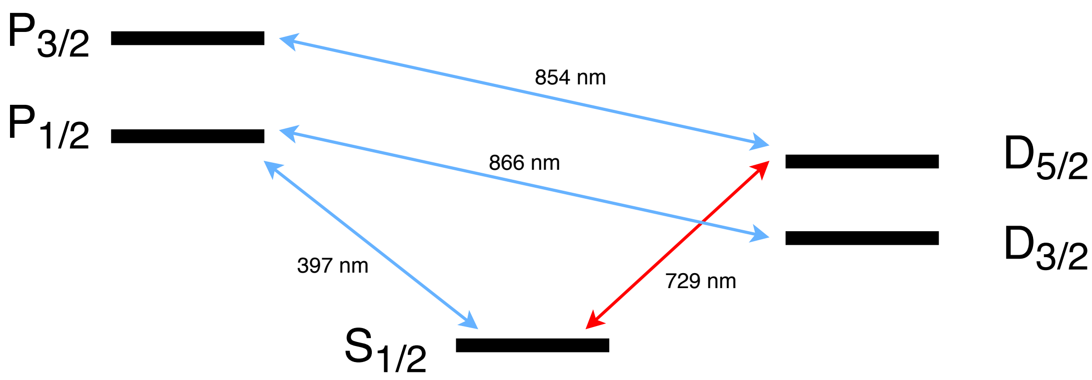

Figure 1.1: Energy levels in $^{40}Ca^{+}$ and the optical transitions between them. Regarding the notation, the letter indicates the occupied orbital (s, p, d or f) and the fraction indicates the total spin $j = l + s$ of the state. The dipole transition driven with a laser at 397 nm is used for Doppler cooling and fluorescence detection, with a repumper at 866 nm. The $S_{1/2}$ to $D_{5/2}$ transition is forbidden by the selection rules, and is a cause for the reasonable long lifetime of the state $D_{5/2}$ [Kie15, Hom17].

order to make an electron jump from $S_{1/2}$ to the $D_{5/2}$ state it is necessary to use a laser of the same wavelength. This is the final advantage of the $^{40}Ca^{+}$ ion: this wavelength corresponds to light in the visible part of the electromagnetic spectrum. Lasers with frequencies in this region are more easily obtainable, and the whole beam alignment process becomes easier and safer, since it is possible to see where the light is going. The main challenge lies in the stability of the laser light used: small variations in frequency and phase of the laser will ultimately broaden its spectrum. Attempting to control the optical transition with an impure laser beam results in loss of coherence in the quantum states, and in the worst case, the escape of the ion from the trap. Given that the beam must be delivered into the vacuum chamber by an optical fiber, the only choice left is to design a system that cancels the phase noise induced by the latter.

1.2 Laser generation system

The fiber noise cancellation setup is one component of a larger laser generation system. An overview is shown in figure 1.2. The laser light is generated by a TOPTICA laser diode, at the lower level, and passes through a cavity for the mode selection: the side frequencies are suppressed, and the faint beam transmitted goes to the diode injection setup, where the light intensity is amplified. The beam then travels through the periscope to the upper level, where it enters a tapered amplifier for a second intensity amplification. The beam exits the amplifier, and arrives at the beam splitters, where the beam gets split into three. Each beam enters a different fiber noise cancellation setup (labelled as 1-3 in the figure). With three independent setups, it is possible to supply three different experiments with stable, monochromatic laser light.

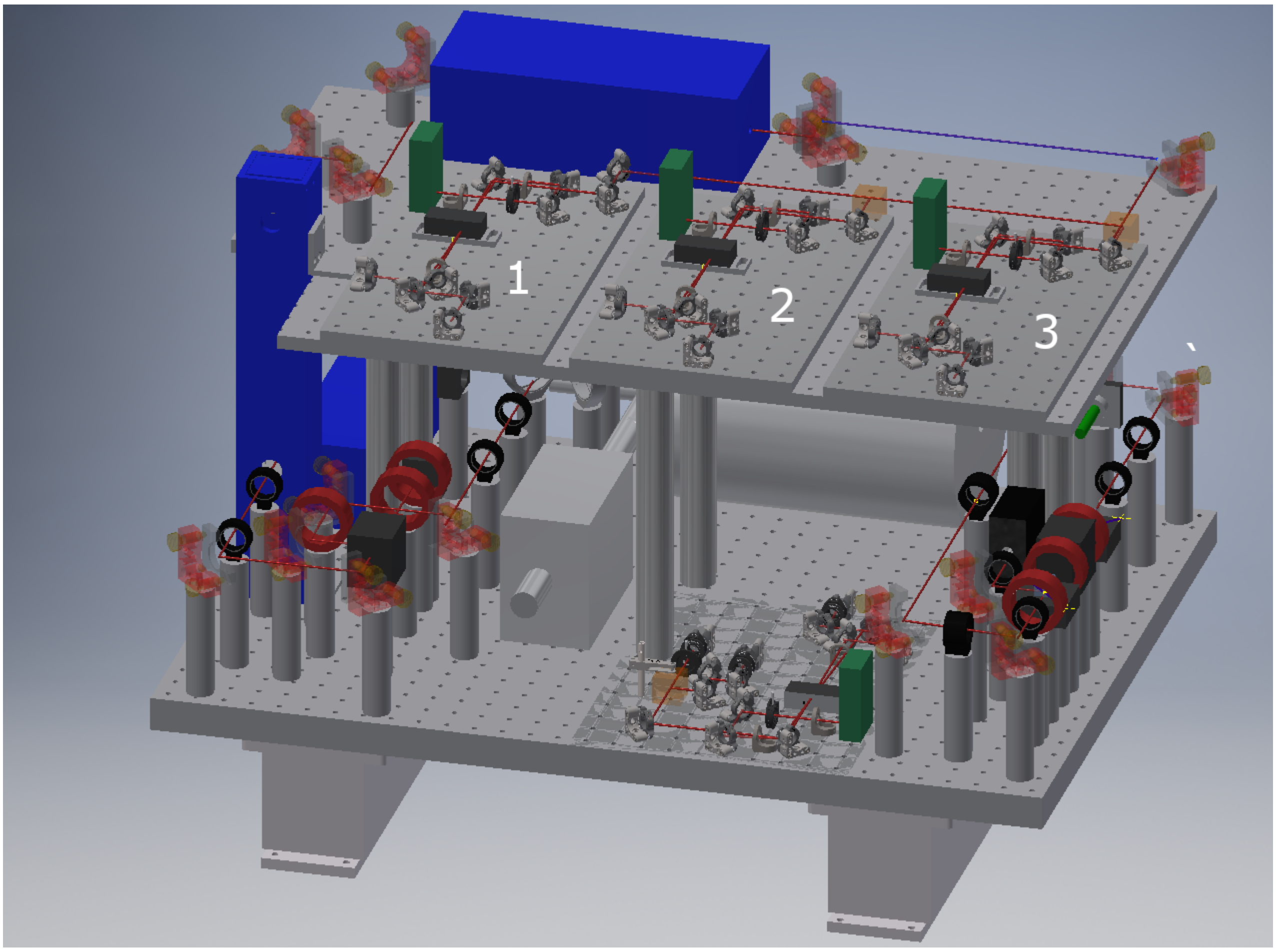

Figure 1.2: Complete view of the laser generation system. The laser beam is generated by a diode at the lower level, and then passes through a cavity for the mode selection. It then enters a diode injection setup, where the first intensity amplification takes place. With the help of a periscope it reaches the upper level, where it gets further amplified with a tapered amplifier. By the use of beam splitters, the beam is sent to three independent fiber noise cancellation setups, which are the three boards above labelled with numbers 1-3. With three independent setups, it is possible to supply three different experiments with stable, monochromatic laser light.

Chapter 2

Theoretical background

2.1 Optical fibers

An optical fiber is a cylindrical dielectric waveguide made of low-loss materials such as silica glass. It has a central core with refractive index n_1 in which the light is guided, embedded in an outer cladding of slightly lower refractive index n_2, see figure 2.1a. Light rays incident on the core-cladding boundary

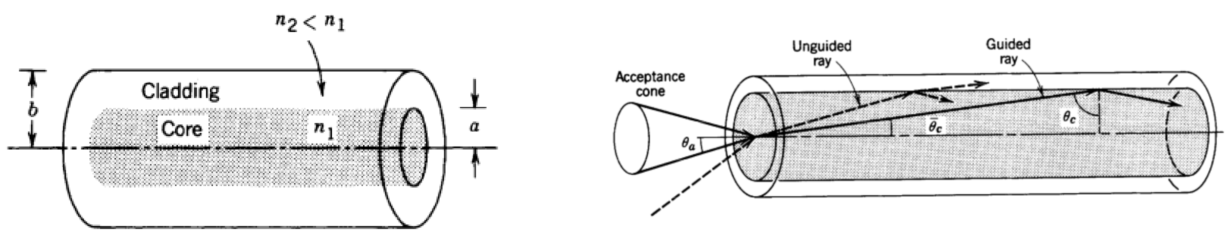

(a) Section of an optical fiber.

(b) Maximum acceptance angle.

Figure 2.1: General properties of optical fibers [ST91].

at angles smaller than the critical angle undergo total internal reflection and are guided through the core without refraction. Rays of greater inclination to the fiber axis lose part of their power into the cladding at each reflection and are not guided, as shown in figure 2.1b. Thus, one can define the maximum acceptance angle $\theta_a = \arcsin(\sqrt{n_1^2 - n_2^2})$. One can further distinguish between PC and APC fiber connectors, see figure 2.2; in PC or UPC (Polished) connectors, due to the end of the fiber being perpendicular to the light path, a portion of the light coming from the fiber is reflected back into the source (the typical optical return loss in the fibers used is 50 dB according to the specifications sheet [Tho18a]). In APC (Angle-Polished) connectors, the end of the fiber is tilted at an angle α (typically $\approx 8^o$) which is greater than the acceptance angle θ_a to avoid the back reflection. APC connectors are useful in circuitry where some of the optical components are sensitive to external oscillations; the noise added from the back reflections might interfere in the setup and thus affect the overall performance. In this setup however, we are interested in getting the reflection at the end of the fiber in order to measure its induced phase shift.

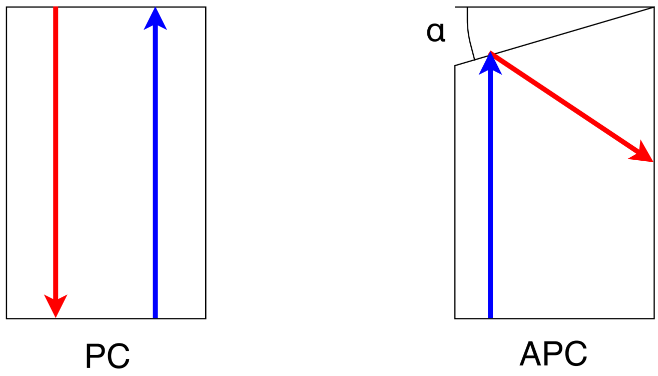

Figure 2.2: Comparison between polished (PC) and angle-polished (APC) connectors. In the former, a small portion of the incoming beam (blue arrow) is reflected back (red arrow) into the source. In the other connector, on the other hand, has the end tilted at an angle α (typically $\approx 8^o$) such that the back reflection is directed to inner wall and is not guided to the other end of the fiber [Tho18a, Tho18b].

2.2 Optical phase noise in optical fibers

A free electromagnetic wave polarized in the z-axis travelling along the x-axis can be described by the equation:

$$E_x = 0, \quad E_y = 0, \quad E_z = E_0 \cos(kx - \omega t + \varphi_0), \tag{2.1}$$

where E_0 is the field amplitude, k is the magnitude of the wave vector, ω is the angular frequency and φ_0 is a phase (from now on only the z-component is regarded). An electromagnetic wave that enters a fiber leaves the other side with an extra phase φ' (which may also be zero). In order to calculate φ', it is necessary to compute the optical path length OPL of the fiber:

$$OPL = \int_\gamma n(\mathbf{r})\ \mathrm{ds}. \tag{2.2}$$

The phase added by the fiber φ is equal to $OPL \cdot k_f$, where k_f is the wave vector inside the fiber. Due to small temperature and pressure changes, the optical path length may alter during time, such that the electromagnetic field after the fiber is

$$E_z = E_0 \cos(kx - \omega t + \varphi_0 + \varphi_\varepsilon(t)), \tag{2.3}$$

and the phase $\varphi_\varepsilon(t)$. The fluctuation of $\varphi_\varepsilon(t)$ over time may broaden the laser spectrum and ultimately reduce coherence.

Suppose the beam at the end of the fiber is partially reflected back and goes through the latter towards the beginning, as shown in figure 2.3 (this can be easily achieved using optical fibers with PC connectors). The beam enters the fiber with a phase φ_0, receives a phase $\varphi_\varepsilon(t)$ when travelling to the right end, gets reflected, receives a second phase $\varphi_\varepsilon(t)$ and exits on the left end. If the two beams are overlapped, they give a total average intensity I_{total} of:

$$\begin{aligned} I_{total} &= I_{incoming} + I_{reflected} + 2\sqrt{I_{incoming} \cdot I_{reflected}} \cdot \cos\left(\Delta\omega \cdot t + (\varphi_{reflected} - \varphi_{incoming})\right), & (2.4)\\ &= I_{incoming} + I_{reflected} + 2\sqrt{I_{incoming} \cdot I_{reflected}} \cdot \cos\left(2\varphi_\varepsilon(t)\right), & (2.5)\end{aligned}$$

where $I_{incoming}$ and $I_{reflected}$ are the average intensities of the individual beams, and $\varphi_{incoming}$ and $\varphi_{reflected}$ are the overall phases of the beam and $\Delta\omega = \omega_{reflected} - \omega_{incoming}$. Given that fiber does not cause any frequency shift, $\Delta\omega = 0$, and the second term becomes $\varphi_{reflected} - \varphi_{incoming} = \varphi_0 + 2\varphi_\varepsilon(t) - \varphi_0 = 2\varphi_\varepsilon(t)$.

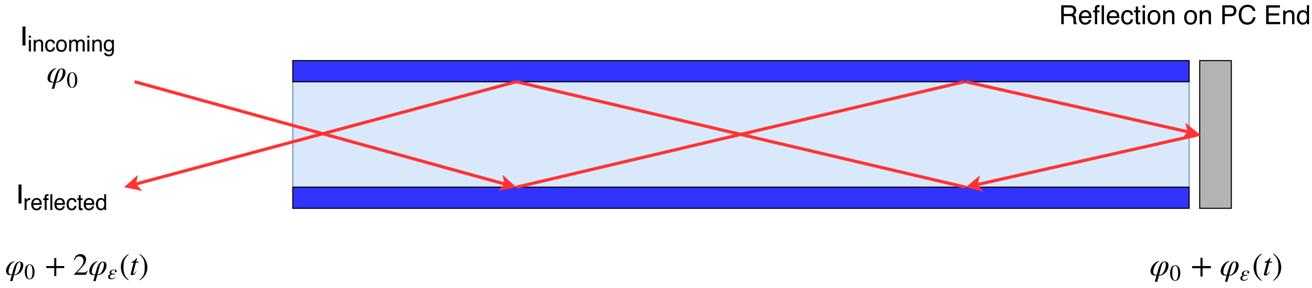

Figure 2.3: Optical fiber with counter-propagating beams. The incoming beam has an average intensity $I_{incoming}$, and enters the fiber with a phase φ_0. The transit through the fiber adds a phase $\varphi_\varepsilon(t)$ to the beam, which gets reflected at the other end. The beam exits the fiber where it entered, with an overall phase $\varphi_0 + 2\varphi_\varepsilon(t)$ and an average intensity $I_{reflected}$, with no frequency shift [Opp15, ST91].

2.3 The Acousto-Optic Modulator (AOM)

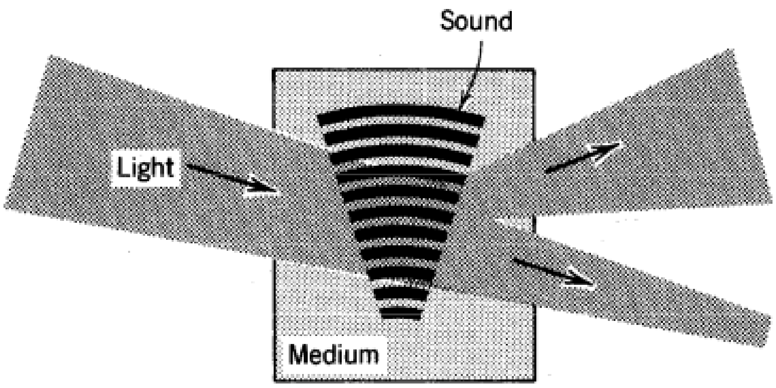

Figure 2.4: Scheme for positive first order diffraction in an AOM [ST91]. The sound waves contract and expand the crystal inside the AOM, such that the index of refraction n ceases to be homogeneous. Because the variations are periodic in time and space, a portion of the incoming light experiences a first order diffraction, which in the figure is the upper right beam.

An acousto-optic modulator (AOM) is a device whose key component is a piezo-electric transducer. By driving the latter with sound waves, the contractions and expansions will alter the dielectric tensor inside the crystal attached to it, which works as an interacting medium. If one also shines a laser beam, since the optical path now varies with time, one can phase-modulate the beam. The light is diffracted into several orders, as shown in figure 2.4. Since optical frequencies are much greater than acoustic frequencies, the variations of the refractive index in a medium perturbed by sound are usually very slow in comparison with an optical period. There are therefore two significantly different time scales for light and sound. As a consequence, it is possible to use an adiabatic approach in which the optical propagation problem is solved separately at every instant of time during the relatively slow course of the acoustic cycle, always treating the material as if it were a static (frozen) inhomogeneous medium. Suppose the strain is given by

$$s(x,t) = S_0 \cos(\Omega t - qx), \tag{2.6}$$

where Ω and q are, respectively, the angular frequency and the wave number of the sound wave, which propagates with velocity v_s. Then the refractive index has the form

$$n(x,t) = n - \Delta n_0 \cos(\Omega t - qx), \tag{2.7}$$

$$\Delta n_0 = \frac{1}{2}\mathfrak{p} n^3 S_0, \tag{2.8}$$

where n is the index of refraction in unperturbed state, and $\mathfrak{p}$ is the photoelastic constant (dependent on material). To determine the amplitude of the reflected wave, one can use the adiabatic approach

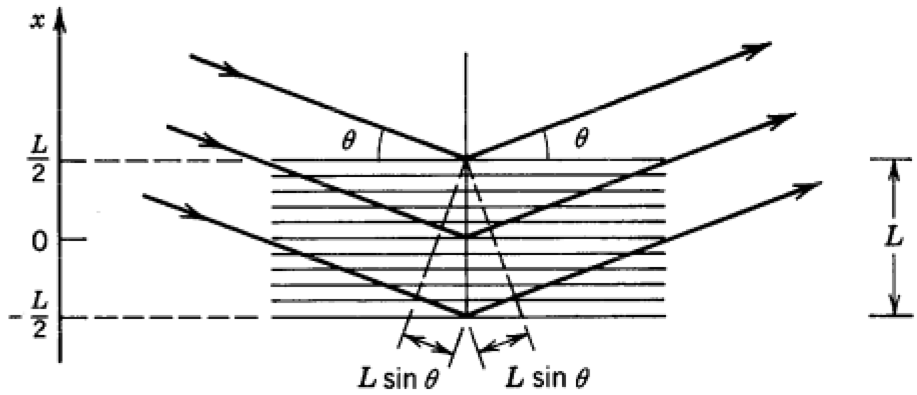

Figure 2.5: Bragg reflections from layers in an inhomogeneous medium [ST91]. The lines perpendicular to the x axis are the peaks of the index of refraction inside the medium, and correspond to the maxima of equation 2.7. The arrows correspond to the path followed by the diffracted photons.

and divide the medium into incremental planar layers orthogonal to the x-axis. Suppose the incident optical plane wave has a wave vector $\vec{\mathbf{k}}$ and an angular frequency ω. Let also $k = |\vec{\mathbf{k}}|$. This wave is partially reflected at each layer because of the refractive-index change. It is also assumed that the reflectance is sufficiently small so that the transmitted light from one layer approximately maintains its original magnitude as it penetrates through the following layers of the medium. If $\Delta r = \frac{dr}{dx}\Delta x$ is the incremental complex amplitude reflectance of the layer at position x, the total complex amplitude reflectance for an overall length L (see figure 2.5) is the sum of all incremental reflectances:

$$r = \int_{\frac{-L}{2}}^{\frac{L}{2}} e^{i2kx\sin(\theta)} \frac{dr}{dx}\, dx. \tag{2.9}$$

The phase factor $e^{i2kx\sin(\theta)}$ must be included, for a wave reflected at x is advanced by a distance of $2x\sin(\theta)$, corresponding to a phase shift of $2kx\sin(\theta)$. Using equation 2.7, one obtains:

$$\frac{dr}{dx} = \frac{dr}{dn}\frac{dn}{dx} = \frac{dr}{dn} q\Delta n_0 \sin(qx - \Omega t) = -\frac{q\Delta n_0 \sin(qx - \Omega t)}{2n\sin^2(\theta)} \tag{2.10}$$

$$\frac{dr}{dn} = -\frac{1}{2n\sin^2(\theta)}. \tag{2.11}$$

The derivative $\frac{dr}{dn}$ is obtained by the use of the Fresnel Equations for reflections in polarized waves [ST91]. It corresponds to the TE (orthogonal) polarization first order approximation; for TM (parallel) polarization, there is an additional factor of $\cos(2\theta)$ in the numerator. Assuming θ to be small enough, $\cos(2\theta) \approx 1$, and the approximation becomes valid for both polarizations. By substituting 2.10 into 2.9, one gets:

$$r = \frac{1}{2} i r' L \cdot \left\{ \text{sinc}\left([q - 2k\sin(\theta)]\frac{L}{2\pi}\right) e^{i\Omega t} - \text{sinc}\left([q + 2k\sin(\theta)]\frac{L}{2\pi}\right) e^{-i\Omega t} \right\}, \tag{2.12}$$

$$r' = \frac{-q}{2n\sin^2(\theta)}\Delta n_0, \tag{2.13}$$

where $\mathrm{sinc}(x) = \frac{\sin(\pi x)}{\pi x}$. This function has two significant maxima: $2k\sin(\theta) = \pm q$ (if L is large enough, then the subsequent maxima are negligible). From this one gets the Bragg conditions for positive and negative first order diffractions. Since the angular frequency of light is ω (i.e. $E \propto \exp(i\omega t)$), the reflected waves $rE \propto \exp(i(\omega \pm \Omega)t)$ have angular frequencies $\omega_{s,\pm 1} = \omega \pm \Omega$ for the positive and negative first order diffractions. The respective wave vectors are $\vec{\mathbf{k}}_{s,\pm 1} = \vec{\mathbf{k}} \pm \vec{\mathbf{q}}$ ($\vec{\mathbf{k}}$ is the wave vector of the light wave and $\vec{\mathbf{q}}$ is wave vector of the sound wave). In conclusion there are two significant diffractions at angles $\theta_{\pm} = \pm \arcsin(\frac{q}{2k})$, each one with a frequency shift and a corresponding phase shift [LYY+05].

The model used is the ATM-2001A22 by IntraAction Corp. [Int13]. It can also be used as an amplitude modulator or a beam deflector. The piezoelectric transducers used to generate the longitudinal RF-frequency acoustic waves are made of Lithium Niobate ($LiNbO_3$) and the interaction medium is made of crystal Tellurium Dioxide (TeO_2). The RF center frequency of operation is 200 MHz, and the height of the sound field (active aperture) is 1 mm. The TeO_2 optical surfaces are coated with a multi-layer dielectric anti-reflection coating. The acoustic velocity inside the medium is $v = 4.26 \cdot 10^3$ m s^{-1}. The first order diffraction efficiency η is defined as:

$$\eta = \frac{I_1}{I}, \tag{2.14}$$

where I_1 and I are the the beam intensity diffracted in first order and the incident beam intensity respectively. The maximum efficiency η_{max} is also dependent on the RF-input power and the wavelength of light used:

$$\eta = \sin^2\left(2.22 \cdot \sqrt{\frac{L}{H} \cdot \frac{M_2 P_a}{\lambda^2}}\right), \tag{2.15}$$

where P_a is the acoustic power, M_2 is the acousto-optic interaction figure of merit, L/H is the sound field length to height aspect ratio and λ is the wavelength of the laser beam. Since the efficiency is a square sine function, with the corresponding maxima at $k\pi,\ k \in \mathbb{Z}$, the RF-power can be optimized for optical wavelengths different from the test wavelength by ensuring the condition:

$$2.22 \cdot \sqrt{\frac{L}{H} \cdot \frac{M_2 P_a}{\lambda^2}} = k\pi, \qquad k \in \mathbb{Z}. \tag{2.16}$$

Given that L/H and M_2 are independent of the acoustic power and optical wavelength, equation 2.16 simplifies to the condition:

$$\frac{P_1}{P_2} = k\left(\frac{\lambda_1}{\lambda_2}\right)^2, \qquad k \in \mathbb{N}, \tag{2.17}$$

where λ_1 is the wavelength of laser light used, P_1 is the desired RF-power, and P_2 and λ_2 are a combination of RF-power and light wavelength that satisfy the condition 2.16, thus yielding a maximum efficiency in equation 2.15. One must be aware that it is possible to overdrive the modulator resulting in a decreased diffraction efficiency. From the specification sheet it is known that the device used yields under optimal conditions a first order diffraction efficiency of 80 % with the RF-Input at 0.48 W (26.81 dBm) and a 632.8 nm laser light (see Appendix B). By choosing $k = 1$, the optimal RF-power P_{729} for laser light of 729 nm wavelength is $P_{729} = 0.637$ W (28.041 dBm).

Chapter 3

Experimental setup

3.1 Methodology

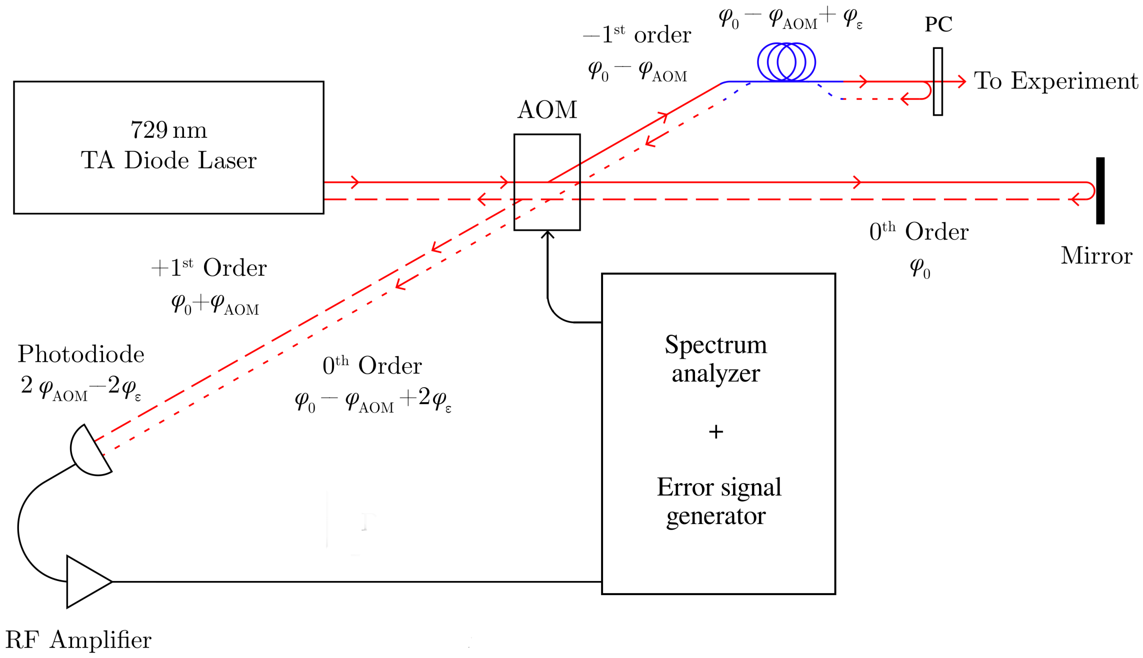

Figure 3.1: General setup of the experiment, adapted from [Opp15]. The beam is generated on the TA Diode Laser, and goes through the AOM where it gets diffracted. The back reflections meet in the photodiode, whose output signal is fed into the error signal generator. The latter tunes the RF-input of the AOM such that the photocurrent in the photodiode remains constant.

The setup is shown in figure 3.1. The beam is generated in the diode laser, with an optical frequency ω, and passes through the acousto-optic modulator (AOM) (which is being driven by a RF-signal with frequency Ω) with an initial phase of φ_0. From section 2.3 it is known that positive and negative refractions at the AOM receive an extra phase of $\pm\varphi_{AOM}$ and a frequency shift of $\pm\Omega$; zeroth order transmissions do not receive any kind of phase [LYY$^+$05]. The -1st order reflection is diverted to the fiber, receives a frequency shift of $-\Omega$ and a phase $-\varphi_{AOM}$, whereas the zeroth order is conducted to a mirror. The $+1$st order from the reflection of the zeroth order is finally directed into a photodiode, with an optical frequency $\omega_+ = \omega + \Omega$ and a phase of $\varphi_0 + \varphi_{AOM}$. The -1st order goes through the fiber (blue cable), is reflected partially at the PC end of the fiber, and while the transmitted beam goes to the experiment, the reflection comes back. The latter goes through the AOM without experiencing any diffraction, as it is not properly aligned, and arrives at the photodiode, with a phase of $\varphi_0 - \varphi_{AOM} + 2\varphi_\varepsilon(t)$ (in the figure $\varphi_0 - \varphi_{AOM} + 2\varphi_\varepsilon$) and a frequency $\omega_- = \omega - \Omega$. Similar to the case in equation 2.4, the overlapping of both beams at the photodiode yields a average intensity I_{PD} of magnitude:

$$I_{PD} = I_{-1st} + I_{0th} + 2\sqrt{I_{-1st} \cdot I_{0th}} \cos\left(\ (\omega_+ - \omega_-)t + 2\varphi_{AOM} - 2\varphi_\varepsilon(t)\ \right), \tag{3.1}$$

$$I_{PD} = I_{-1st} + I_{0th} + 2\sqrt{I_{-1st} \cdot I_{0th}} \cos\left(\ 2\Omega t + 2\varphi_{AOM} - 2\varphi_\varepsilon(t)\ \right), \tag{3.2}$$

where I_{-1st} and I_{0th} are the average intensities of the respective beams. The laser signal arriving at the photodiode is of the form:

$$\sqrt{I_{PD}} \cos(\omega t + \phi_0), \tag{3.3}$$

where I_{PD} also oscillates with frequency 2Ω. Here it is important to notice that whereas ω is the optical frequency which lies in the THz range, Ω is an RF-frequency that lies in the MHz range. The signal thus, has two significant frequency components, one at 2Ω (which in the AOM used is 400 MHz) and another at ω. What is also important to notice is the presence of $\varphi_\varepsilon(t)$ in equation 3.2, which means that the time fluctuation of the optical path in the fiber also broadens the spectrum of the photodiode's signal. By choosing a photodiode with a detection bandwidth centered at 2Ω and that is wide enough to detect small variations in the AOM frequency yet does not extend to the GHz region, the signal output of the photodiode has only one significant frequency component, namely 2Ω. In order to reduce the spectral width, it is necessary to tune the AOM such that:

$$\varphi_\varepsilon(t) = \varphi_{AOM}. \tag{3.4}$$

Given that φ_{AOM} is dependent on the frequency of the sound wave [LYY+05], it is possible to generate an error RF-signal which reduces the spectral width of the photodiode signal. By keeping the feedback loop running, any variation of $\varphi_\varepsilon(t)$ over time broadens the spectrum of the photodiode signal, which is then used by the POISON electronic circuit [Opp15] to adjust the error signal such that the identity $\varphi_\varepsilon(t) = \varphi_{AOM}$ remains valid, and the spectral width of the photodiode's signal remains narrow. Oddly enough, this actually solves the initial problem: the laser beam after PC in figure 3.1 (which is the one that actually goes to the experiment) has a overall phase:

$$\varphi_{exp} = \varphi_0 + \varphi_\varepsilon(t) - \varphi_{AOM}. \tag{3.5}$$

The term φ_0 is a constant phase picked up by travelling from the laser source to the experiment that does not vary over time. If the condition $\varphi_\varepsilon(t) = \varphi_{AOM}$ holds, than the overall phase at the end φ_{exp} is equal to φ_0 and thus constant in time. This setup is only effective for which the phase noise of the fiber is slow compared to the transit time of light in the fiber ($\approx 0.125\ \mu$s), such that the phase does not vary significantly during the transit of the laser beam. In the given setup this means that only phase noises with variations slower than 2 kHz can be effectively suppressed [Opp15].

3.2 Compact setup

A diagram for the optical setup is shown in figure 3.3. The black and the green boxes are the AOM and photodiode (PD) respectively; they are both connected to the error signal generator. The initial laser beam (red) comes from the bottom, and is directed by mirrors M1A and M1B to the AOM, where it gets diffracted into the zeroth order transmission and the negative first order diffraction. The zeroth order transmission (red, above the AOM) is directed into mirror M2A and then reflected back by mirror M2B. The negative first order diffraction (blue, above the AOM) is directed via mirrors M3A and M3B into the fiber coupler FC2, which is connected to the fiber that delivers the beam to the ion trap. Using APC to PC-Fibers (fibers in which one of the connectors is PC and the other is APC, see figure 2.2), it is possible to connect the APC connector to the fiber coupler FC2 and the PC end at the vacuum chamber. This arrangement ensures that a small portion of the beam is reflected back

(a) Front view. (b) Top view. (c) Back view.

Figure 3.2: Front, top and back views of the Polaris© K05 mirror mount manufactured by ThorLabs Inc. [Tho15]. The mirror is placed in the hole shown in the back and front views. The hole shown in the top view is used to fix the mirror mount to the optical table.

on the PC end following the blue path on reverse until the AOM (the reflection before the fiber is not guided back to the AOM because of the APC connector). This portion passes through the AOM with no first order diffraction because of misalignment (blue, below the AOM) and is directed via mirrors M4A and M4B into the photodiode. The zeroth order reflection from mirror M2B is diffracted by the AOM into the negative first order, and follows the blue path into the photodiode, and overlaps with the reflection from the fiber. The lenses L1A, L1B and L3 are purely for focusing, as the AOM diffraction efficiency has a small dependence on width of the beam and in the case of L3 the photodiode has a small collection One is free to choose their focal lengths, as long as L1A and L1B have the same. The specifications of the board, together with the exact positions of the optical elements are given in Appendix C.

It is of special interest the maximization of the laser power into the ion trap, meaning that the optical devices need to be properly aligned. The objective of the alignment is to maximize the power of the laser beam being delivered into the experiment at the fiber coupler FC2 and make sure that the back reflections (blue beam, below the AOM in figure 3.3) are directed into the photodiode PD, with maximum power. The AOM first-order diffraction efficiency η in this case is given by:

$$\eta = \frac{P_1}{P_1 + P_0}, \tag{3.6}$$

where P_1 is the power from the beam diffracted at negative first order which is measured between mirrors M3A and M3B and P_0 is the power for the zeroth order, measured between mirrors M2A and M2B. It is assumed that the power loss in the AOM and the higher order scatterings are negligible. According to the instruction manual [Int13], the model used has, under optimal conditions, a first-order efficiency of 80 %.

The mirrors and mirror mounts are manufactured by ThorLabs Inc. [Tho15]. The Polaris© half-inch optics series allows precise alignment of mirror due to its mounts. They are made from stainless steel, since it has a low thermal expansion coefficient, and are screwed down to the board, which gives them mechanical stability, since they cannot be moved. The three screws at the edges, however, allow the user to rotate the mount vertically and horizontally, ensuring a fine calibration of the beam, with an average angular displacement of 11 milliradians per revolution of the screw. This is crucial for the alignment, as the light transmission in the AOM and the fiber are extremely sensitive with respect to the beam angle of incidence.

3.3 Alignment process

The alignment process is a crucial step for the fiber noise cancellation. There is only one main objective: ensure that the laser beam, its reflections and diffractions pass through all the components in the way described in the previous section and maximize the incident power in the vacuum chamber. The process can be summarized in 5 steps:

1. First alignment: the beam coming from the bottom of figure 3.3 is aligned into the AOM by eye such that the zeroth order transmission hits mirror M2A and the negative first order diffraction hits M3A. This must be done using both mirrors M1A and M1B to walk the beam.

2. First fine alignment: a power meter is placed between M3A and M3B. A fine alignment is then performed with M1A and M1B such that the measured photocurrent is maximized. A successful completion of this step requires that the modulator's RF-frequency and power must be at a setting such that the diffraction efficiency is optimized (see section 2.3 for further details).

3. Fiber coupling and its back reflection: the laser pen is placed at the end of the fiber and turned on, generating a reference beam of the same wavelength. The first eye alignment is made: by only adjusting M3A and M3B, the negative first order diffraction beam is tilted such that it overlaps with the reference beam at any point between FC2 and the AOM. The power meter is then placed at other end of the fiber, and the fine alignment is made such that there is maximal power at the other end. As soon as this is achieved, a paper is placed between M2A and M2B, blocking the back reflection originating from the latter mirror. The power meter is disconnected from the fiber, and the back reflection from the fiber is then aligned by eye using mirrors M3A and M3B such that it passes through the AOM and hits mirror M4A. In extreme cases where the last step becomes extremely difficult, one may also adjust the fiber coupler's mount FC2 and start the whole fiber coupling process again.

4. Alignment of the zeroth order back reflections: using mirrors M2A and M2B, the zeroth order is reflected back into the AOM. As the back reflection has an optimal incidence angle, it also splits into a zeroth order and a positive first order diffraction. The latter is directed to mirror M4A.

5. Photodiode: using mirrors M4A and M4B, the two back reflections are aligned such that they enter the photodiode PD. A paper is placed between M2A and M2B to measure the power from the fiber back reflection. The paper is then placed between M3A and M3B and the power from the zeroth order back reflection is then measured.

A more detailed explanation describing the techniques used for the laser alignment is given in Appendix A.

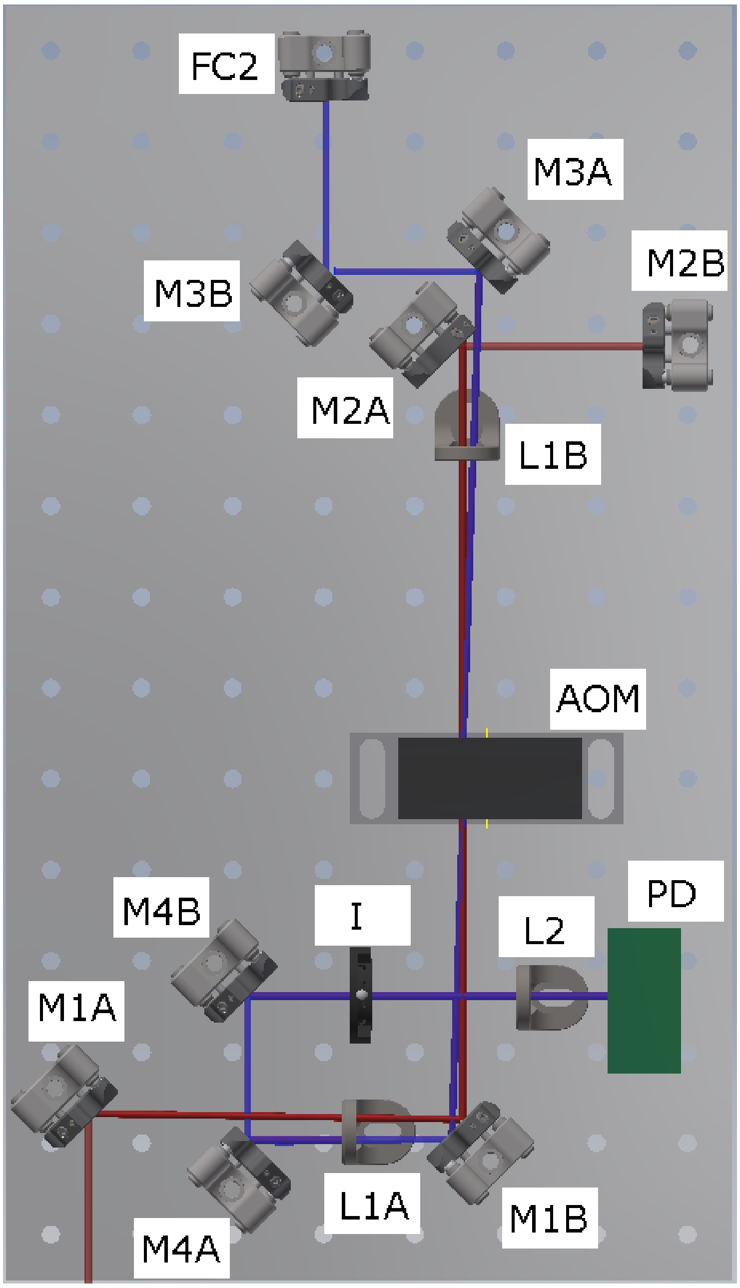

Figure 3.3: Model of the optical table used. The letters M, L, I and FC stand for mirror, lens, iris and fiber coupler (M1A is the Mirror M1A, for example). Each number characterizes an aligning mirror pair or a lens pair, with the exception of the fiber coupler (see Appendix A for further information on aligning pairs). PD is the photodiode and AOM is the acousto-optic modulator. Although not shown, the AOM and the photodiode are connected to the error signal generator. A diagram showing the exact positions of the optical elements, together with the specifications of the board, is given in Appendix C.

Chapter 4

Results

4.1 Power measurements

There are six power measurements to be performed in the compact setup shown in figure 3.3. The first two are the initial beam and the fiber input, which are, respectively, the one that comes from the bottom left and the one which is the beam between M3B and FC2. They are both necessary to determine the overall attenuation of the fiber noise cancellation setup. The second two are the intensities of the zeroth and negative first order diffractions of the AOM, both required to calculate the AOM efficiency defined in equation 3.6. The zeroth order intensity is measured between M2A and M2B, whereas the negative first order intensity is measured between M3A and M3B. Given that the mirrors used show negligible attenuation, the power measurement for the negative first order diffraction (laser beam between M3A and M3B) yields the same result of the fiber input (laser beam between M3B and FC2). The third duo is composed by the intensities of the back reflections on the photodiode, measured between M4B and I. These are necessary for a suitable choice of a photodiode: it must be sensitive enough to detect small variations in the laser signal yet be able to withstand the laser intensity without damage. The laser power after the fiber which starts at FC2 is also measured, since it corresponds to the actual available laser power for the experiment and it is necessary for the calculation of the effective attenuation of the setup combined with the fiber. The AOM diffraction efficiency η, according to

Table 4.1: Laser power measurements. All of the measurements are performed with the same power meter using laser light centered at 729 nm. All of the measurements are taken with the lens pair L1A and L1B removed from the setup. RF-frequency used: 200 MHz, RF-power used: 28.041 dBm.

Point of measurement	**Position in figure 3.3**	**Power**
Incident beam	before M1A	2.898 mW
AOM 0th order	between mirrors M2A and M2B	0.740 mW
AOM -1st order / Fiber input	between mirrors M3A and M3B	1.840 mW
Output after fiber	not in figure	1.270 mW
0th order back reflection	between mirror M4B and iris I (beam blocker placed between M3B and FC2)	0.362 mW
1st order back reflection	between mirror M4B and iris I (beam blocker placed between M2A and M2B)	14.5-15.0 μW

equation 3.6, lies at 71.3 %, which is less than the 80% found in the manual [Int13]. The reasons for the discrepancy may lie in the beam shape, polarization and width. The second problem becomes evident by taking a closer look in the theoretical derivation of the angle of diffraction: the term in equation 2.11 is strongly dependent on the type of polarization used, and the differently polarized components of light might be diffracted by different angles. With regards to the beam width, this problem can be solved by the use of appropriate lenses placed at L1A and L1B; in the setup used both had a focal

length of 100.0 mm [Tho09], yielding a beam width of 0.24 mm at the AOM, which actually reduced the AOM peak efficiency to 30 %, and had to be removed. From the manual it is known that the device used yields an efficiency η of 80% with a beam width of 0.8 mm (see Appendix B). Given that the beam coming from the fibers has a width of 2.0 mm [Tho18a], a lens with a focal length 185 mm, which yields a beam width of 0.79 mm at the AOM, might increase the diffraction efficiency.

Another important aspect to be analyzed are the maximum and minimum frequencies and RF-powers under which the AOM can be modulated such that there is still a significant laser power after the fiber. Figure 4.1 shows that it is possible to operate within 1 MHz of the center frequency of 200 MHz and still have less than 30% laser power attenuation, whereas figure 4.2 shows it is possible to operate within 2.5 dBm of the optimized power P_{729} and also keep the laser power attenuation below 30%. Although the alignment was made using an RF-signal of 28.041 dBm (which is the theoretical optimized power given by equation 2.17) centered at 200 MHz, the setup is further optimized if the AOM is driven using a stronger signal of 29 dBm centered at 200.4 MHz. A half waveplate attached to a rotation mount is placed between mirror M3B and fiber coupler FC2. The rotation mount is graded, which allows to measure the rotation angle. The fast axis of the half waveplate is located at the 286 degree mark. Figure 4.3 shows the laser power measured after the fiber as a function of the rotation angle of the waveplate. The angle is measured with respect of the vertical axis.

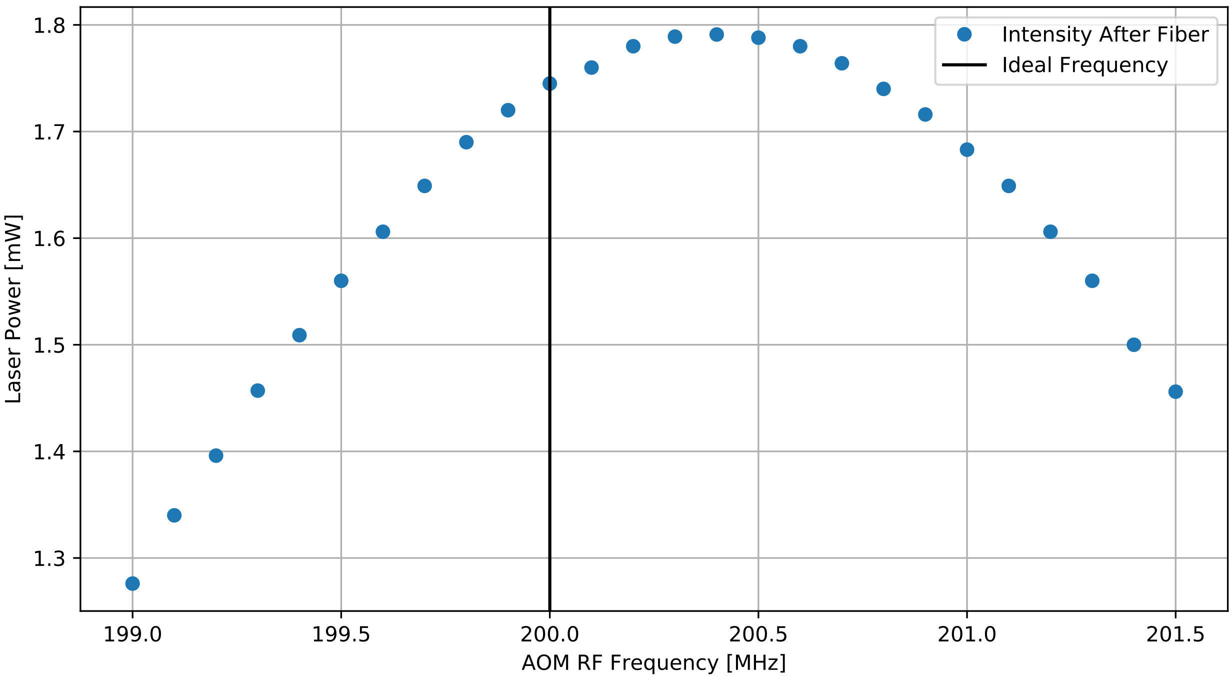

Figure 4.1: Power measured after the fiber as a function of driving frequency of the AOM (RF-power used: 28.041 dBm). Although the alignment was made using an RF-signal centered at 200 MHz, the setup is further optimized if the AOM is driven by a signal centered at 200.4 MHz.

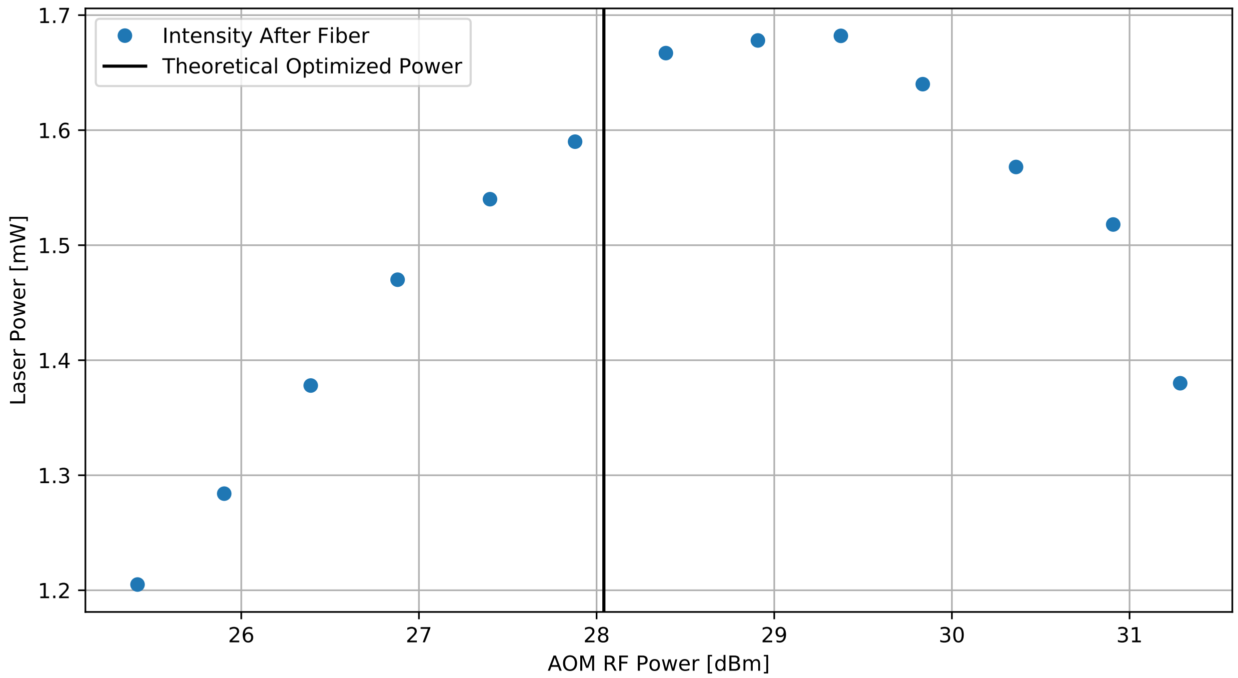

Figure 4.2: Power measured after the fiber as a function of RF-power in the AOM (RF-frequency used: 200 MHz). The vertical line is the theoretical optimized power for the AOM given by equation 2.17, however the setup is optimized if the AOM is driven by a stronger signal of 29 dBm.

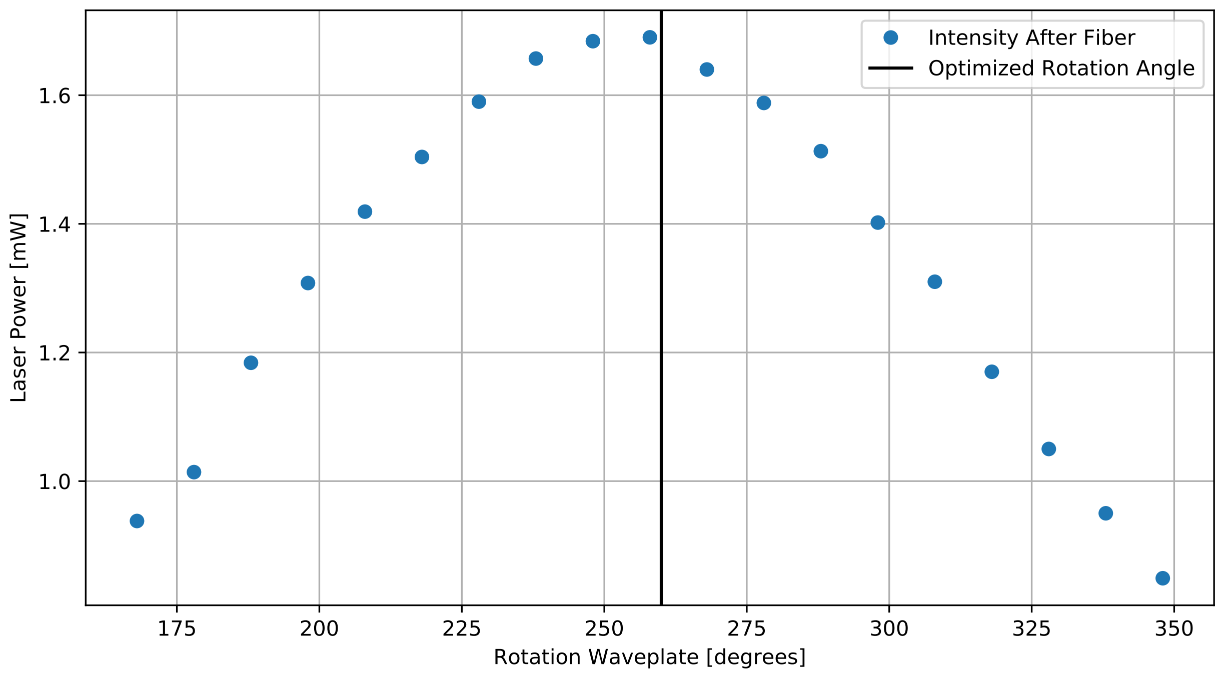

Figure 4.3: Power measured after the fiber as a function of the rotation angle of the half waveplate placed between mirror M3B and fiber coupler FC2. The angle is measured with respect of the vertical axis (RF-frequency used: 200 MHz, RF-power used: 28.041 dBm).

4.2 Photodiode signal

The photodiode is connected to a spectrum analyzer and the measurements are shown in figure 4.4. Contrary to expectation, there are actually three signals being collected:

1. Theoretical signal (or T-Signal): This is the actual signal which comes from the processes explained in section 3.1. It is centered at 400 MHz, and is dependent on the phase noise of the fiber.

2. Noise from the zeroth order reflection (or 0-Noise): It corresponds to the signal registered at the photodiode when a beam blocker is placed between mirror M3B and fiber coupler FC2. This signal is also centered at 400 MHz, yet it does not depend on the phase noise of the fiber

3. Noise from the negative first order reflection (or 1-Noise): It corresponds to the signal registered at the photodiode when a beam blocker is placed between mirrors M2A and M2B. As seen in figure 4.4, it is negligible.

The signal collected by the photodiode when the there are no beam blockers (Raw signal or R-Signal) is simply the sum of the three signals presented above. It is also worth noting that the spectrum analyzer also shows a peak at 200 MHz, even when a beam blocker is placed in front of the photodiode. Given that this peak is also dependent on the AOM RF frequency and power, it is possible to conclude it is a pickup signal from the RF signal generator. By choosing a suitable detection bandwidth in the error signal generator, it can be simply ignored, as it does not affect the fiber noise cancellation process.

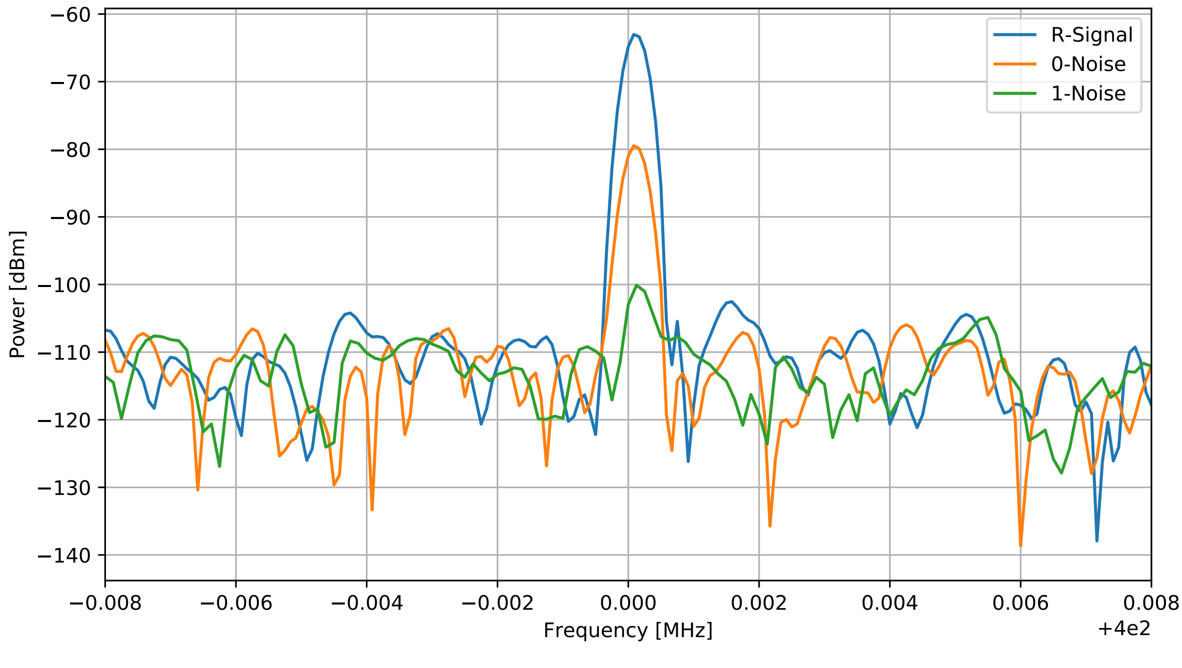

Figure 4.4: Spectra of the signals detected by the photodiode, all centered at 400 MHz. The raw signal (R-Signal) corresponds to the signal when the beam is unblocked. The noise from the zeroth order reflection (0-Noise) is the signal obtained when a beam blocker is placed between M3B and FC2; the noise from the negative first order reflection (or 1-Noise) is the signal obtained when the beam blocker is placed between mirrors M2A and M2B. (RF-frequency used: 200 MHz, RF-power used: 28.041 dBm).

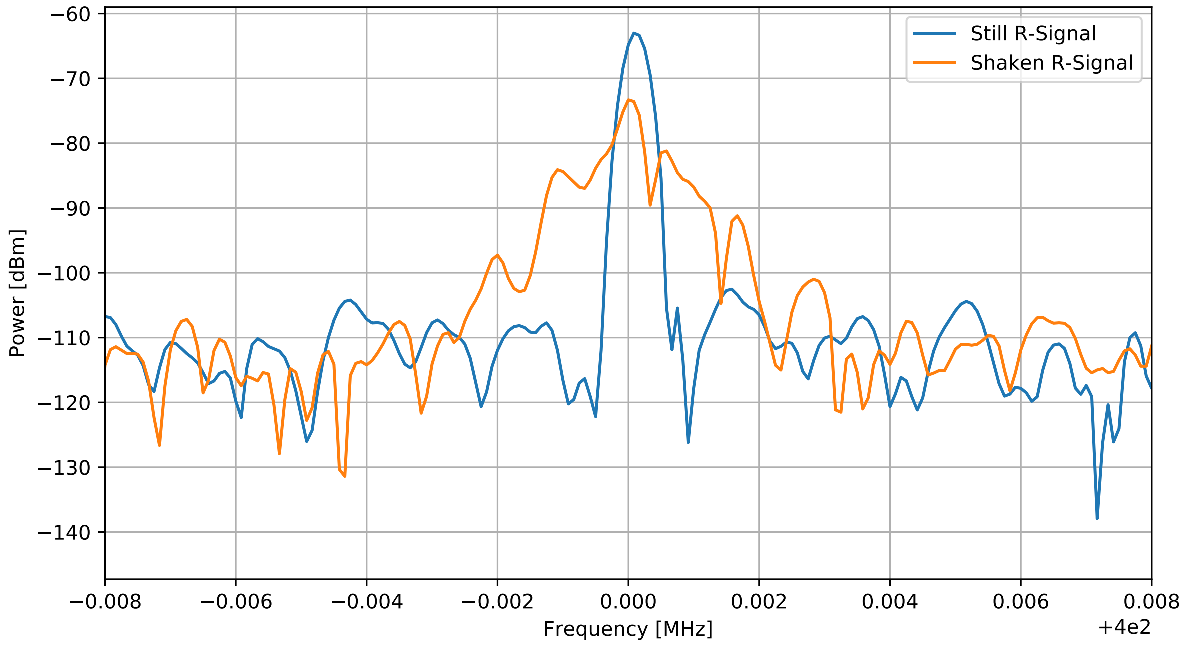

Figure 4.5: Spectra of the R-signals detected by the photodiode, both centered at 400 MHz. In the Still R-Signal spectrum, the fiber is left untouched, whereas in the Shaken R-Signal spectrum, the fiber is gently vibrated manually. The latter signal has a greater spectral width and a peak noise attenuation of 10.3 dB (RF-frequency used: 200 MHz, RF-power used: 28.041 dBm).

The 0-Noise is of particular interest: in theory, it should not exist. The photodiode signal, as shown in equation 3.3, is a beat tone formed by the interference of negative first order reflection from the fiber and the zeroth order reflection from mirror M2B. Given that the former signal is completely attenuated by beam blocker, there are two possible causes for the presence of the 0-Noise:

1. Due to non-trivial reflections in the AOM (which has a highly reflective surface on the inside), a part of the incoming beam is directed back into the photodiode with a frequency shift of $-\Omega$, where $\Omega = 200$ MHz is the RF-frequency driving the AOM. This small reflection overlaps with the zeroth order reflection, which has a frequency shifted by $+\Omega$, thus yielding the beat tone whose spectrum is centered at $2\Omega = 400$ MHz.

2. Due to non-harmonic higher order processes in the AOM, a small portion of zeroth order transmission receives a frequency shift of -2Ω, however its path is not deflected. This beam follows the same path of the zeroth order transmission, and overlaps at the photodiode.

The photodiode is then placed at between mirrors M2A and M2B. Again, a peak at 200 MHz is registered in the spectrum analyzer, even when a beam blocker is placed in front of the photodiode, which again evidences the presence of the pickup signal from the AOM RF-signal generator. More important however, is the presence of a peak at 400 MHz which depends on the back reflected light from the fiber, as shown in figure 4.6. The raw signal is a consequence of the fiber back reflection experiencing a second negative order diffraction; as the beam returns from the fiber coupler FC2, a portion of the beam experiences another negative first order diffraction in the AOM, receiving a second frequency shift of $-\Omega$. The transmitted portion follows a path to the photodiode, whereas the diffracted beam is reflected at the aperture of the AOM and is reflected at mirror M2A. This reflection, which has an optical frequency of $\omega - 2\Omega$, overlaps with the initial zeroth order transmission, which has an optical frequency of ω, thus yielding the beat tone centered at 400 MHz. This explains the power difference in figure 4.6 when the beam blocker is placed between mirror M3B and fiber coupler FC2. It does not explain, however, the existence of the Fiber Block signal.

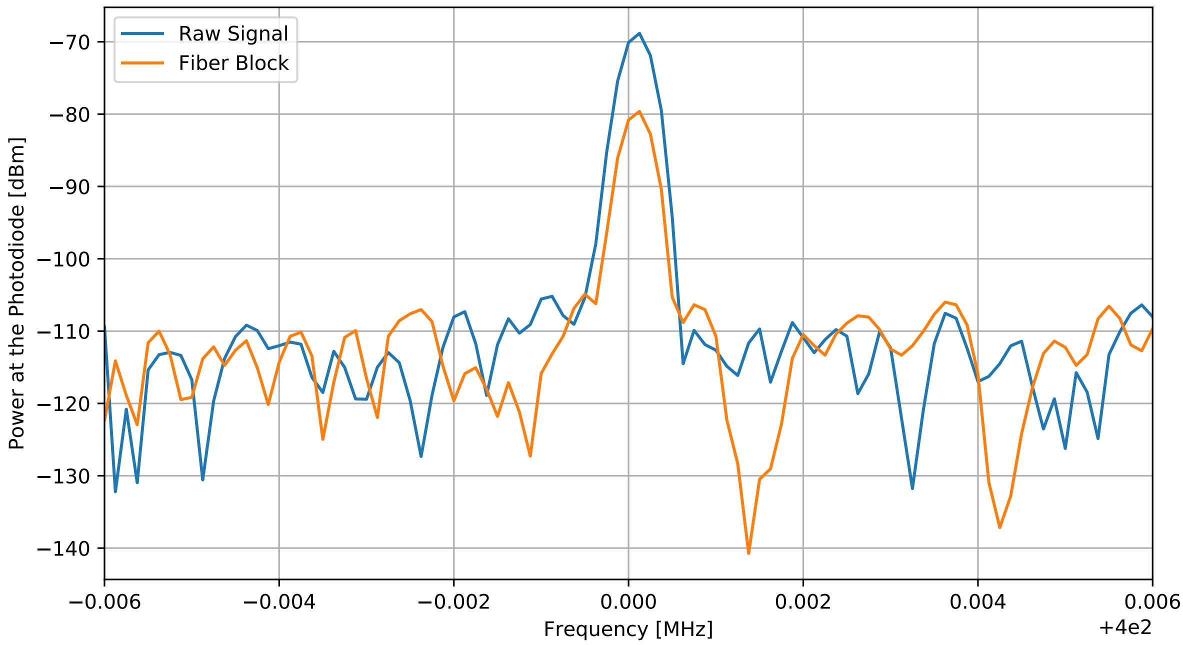

Figure 4.6: Spectra of the signals collected by the photodiode, which is placed between mirrors M2A and M2B, facing the former. The Raw Signal corresponds to the spectrum collected when the setup is completely unblocked, and the Fiber Block signal is the spectrum collected when a beam blocker is placed between mirror M3B and fiber coupler FC2.

Following the approach presented by Oppong [Opp15], it is possible to place a neutral density filter with optical density d between M2A and M2B such that the 0-Noise at the photodiode is completely attenuated. The optimal optical density d is experimentally found to be 10. The resulting signal is also dependent on the vibrations of the fiber, this time with a peak noise attenuation of 7.9 dB, as shown in figure 4.7.

Another important aspect to be analyzed are the maximum and minimum frequencies under which the AOM can be modulated such that there is still a significant signal registered on the photodiode. Given that the spectra are distributions centered at a certain frequency, we are actually interested in the peak to noise ratio (the peak is the power measured at the top of the spectrum of the R-Signal, the noise is defined as the peak of the corresponding 0-Noise). Figures 4.8 and 4.9 show the dependence of the peak to noise ratio as a function of the driving frequency and the RF-power in the AOM. The error bars show the variation of the peak over time (the peak of the 0-Noise does not show visible variation). It is important to notice that the peak of the 0-Noise increases at higher RF-frequencies and lower RF-powers. There are some unstable points (where the peak of the R-Signal varies more than 5 dBm) in figure 4.8, which are located at the ends of the spectrum (199.7 MHz and 200.35 MHz). In figure 4.9, there are some points in which the peak of the R-Signal drops significantly such that the peak ratio to the 0-Signal is less than 4 dB. There are also points where the peak ratio is clearly above 10 dB, and in those cases, the variation over time is reduced below 2.5 dBm. This behaviour is mostly a consequence of the external noise in the fiber coming from the environment.

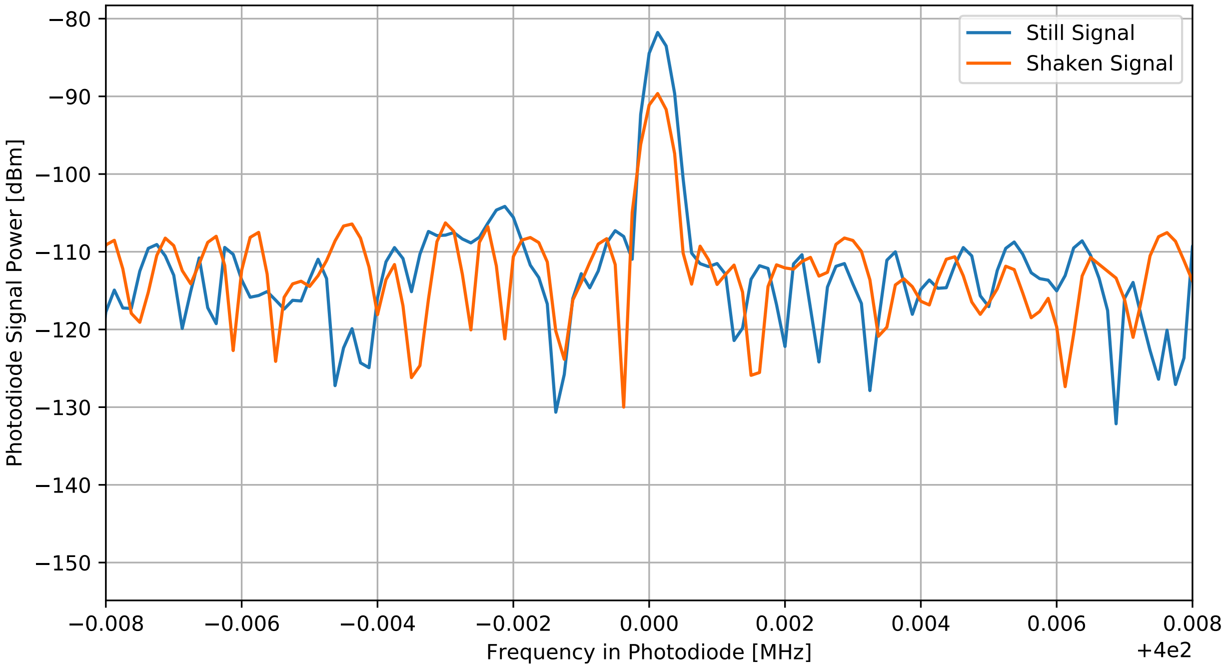

Figure 4.7: Spectra of the signals detected by the photodiode when a neutral density filter of optical density $d = 10$ placed between mirrors M2A and M2B, both centered at 400 MHz. In the Still Signal spectrum, the fiber is left untouched, whereas in the Shaken Signal spectrum, the fiber is gently vibrated manually. The latter signal has a greater spectral width and a peak noise attenuation of 7.9 dB (RF-frequency used: 200 MHz, RF-power used: 28.041 dBm).

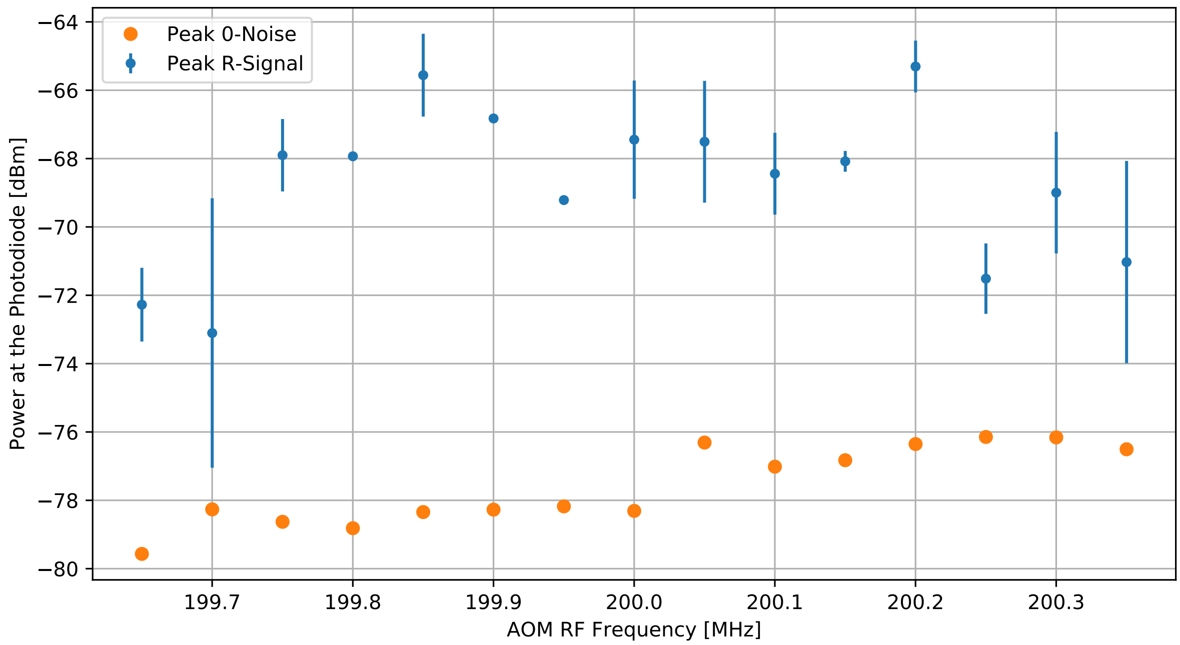

Figure 4.8: Peak of the R-Signal and 0-Noise as a function of the RF-frequency of the AOM (RF-power used: 28.041 dBm).

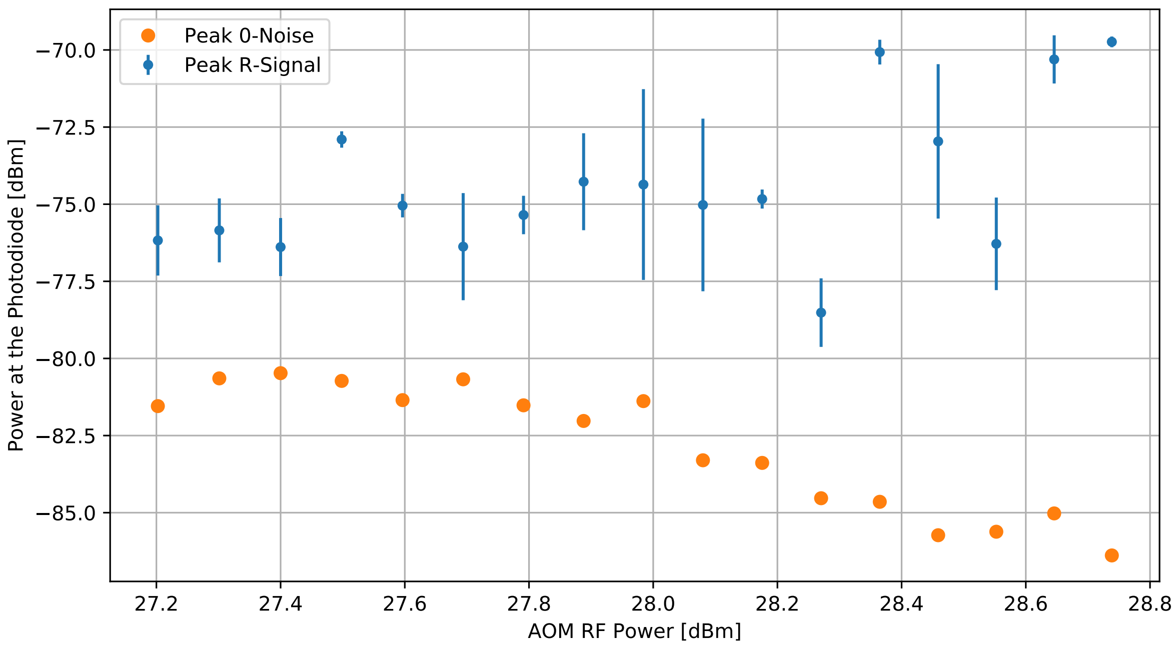

Figure 4.9: Peak of the R-Signal and 0-Noise as a function of RF-power in the AOM (RF-frequency used: 200 MHz).

Chapter 5

Conclusion

5.1 Summary

The compact setup is suitable for the fiber noise cancellation. This is evidenced in the dependence of the spectrum of the photodiode signal with respect to mechanical noise in the fiber. Most importantly, given that the travelling time of the fiber lies in the order of 10^{-7} s, the delay between phase noise in the fiber and the phase noise in the photodiode signal is of the same magnitude, which is a negligible delay for practical purposes. This condition also places an upper limit on the types of noise that can be cancelled: in the conditions used the phase noise frequency must not exceed 2 kHz. This condition ensures that the induced phase does not alter significantly during the transit time of the fiber.

Another important aspect of the setup is the use of half-inch optics. Contrary to more conventional approaches, the mirrors, lenses and subsequent optical devices are at fixed positions in an aluminium plate, which is lighter and softer, yet as rigid as other materials such as steel. Although the setup is harder to align, it offers more mechanical stability, not to mention that it takes less space. Given that this setup is supposed to be used in several different experiments, the additional reliability offered makes the laser one less thing to be worried about in experimental debugging.

The setup is also significantly stable under AOM signal modulations. As shown earlier, the AOM can be operated within 300 kHz of the central frequency or within 0.4 dBm of the optimized power P_{729} and laser power attenuation remains below 30 %. In all of the cases shown, the peak to noise attenuation in the photodiode is at least 2.5 dB, which is clearly distinguishable for an error signal generator.

5.2 Outlook

One of the aspects yet to be analyzed is the phase noise suppression of the fiber provided by the setup, and whether it is as effective as the conventional setups currently used. Theoretically speaking, the cancellation is possible in phase noises with maximum frequency below 2 kHz, which in most cases suffices, as most laboratories are isolated to external interference sources. All in all, it is a promising setup, mostly due to its compactness and reliability.

Chapter 6

Acknowledgements

Firstly, I would like to thank Matthew Grau and Professor Jonathan Home for making the whole semester project possible. I would also like to thank Maciej Malinowski, Roland Matt, Christopher Axline, Robin Oswald, Daniel Kienzler and Matteo Marinelli for the help, patience and the valuable lessons learned; Philipp Verwegen, Martin Stadler, Christa Flühmann, Vlad Negnevitsky, Tanja Behrle, Karan Mehta, Francesco Lancellotti and Thanh Long Nguyen for the good time spent in the office and finally, I would specially like to thank Chiara Decaroli, for the orientation, support and dedication throughout the whole semester project.

Appendix A

Laser beam alignment techniques

The alignment of laser beams is no trivial subject and requires a lot of time and attention. The main issue in this setup, as stated earlier, is the fact that the mirrors and lenses are at fixed positions and can only be tilted to ensure the correct path to be followed. Its implications are simple: an optical setup that requires an extensive first alignment and is less susceptible to mechanical and thermal interference. Given that the laser setups are supposed to be used in several different experiments, the research group has chosen this method in order to avoid future misalignment problems. A good alignment is characterized by no unnecessary loss of laser power, which is equivalent of having maximal photocurrent at the end of the beam path (unnecessary is an important word here since there are several optical devices in which there is a significant loss of laser power even at optimal settings, such as the case of an optical fiber).

The first alignment must be made by eye. It is certainly not the most efficient way, but it is necessary to make sure that the beam is at least going in the right direction. Luckily enough, the necessary laser wavelength is 729 nm, which lies in the visible part of the spectrum. Given that even the reflections in the fiber end must be visible to the naked eye, there is already a minimum laser power requirement at M1A which is experimentally found to be 2.0 mW. This intensity can cause blindness if the beam is directed into the eye. A good solution is to place a piece of paper in front of the beam and follow its trajectory, as the papers do not burn at the current laser power. This also allows one to (roughly) see whether the beam has a elliptic profile which can probably affect the fiber coupling.

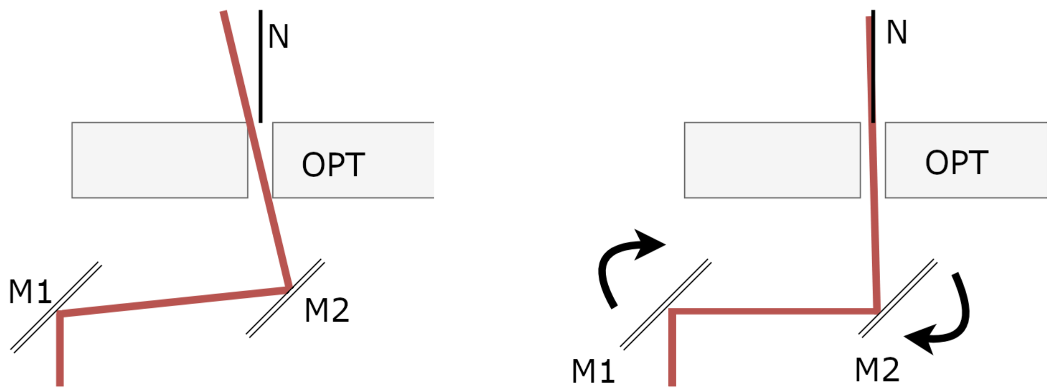

Figure A.1: Walking the beam (red line) using a aligning pair of mirrors, M1 and M2, into an optical device with a narrow aperture, OPT. A beam that exits OPT overlapping with the reference line N has maximal amplitude.

The second major issue in the setup in figure 3.3 is the presence of two optical devices that require the beam to pass through them at a specific point with a certain angle of incidence: the AOM and the fiber coupler. They are also the main components of the setup, which means that the great majority of effort is put into aligning the beam into those two. The first step is understanding how to use the given set of mirrors to accomplish that: in the same figure it is important to notice that some mirrors are labelled as M1A and M1B. This is no coincidence, as each number characterizes an aligning pair: since the mirrors cannot be moved, it is necessary to use a aligning pair to walk the beam in order to get the best results. Suppose the setup in figure A.1 is given. In the left picture, the beam (red line) is certainly aligned by eye: if one puts a paper after the hole, the circular profile appears as in the usual case. The beam, however, is not aligned with the reference line of the aperture (black line labelled as N), and does not come out with the same intensity as the right one. The change in intensity, nevertheless, can be so small that it is not perceivable to the human eye, and this is where the power meter becomes useful: by first placing the latter after the aperture and then rotating one of the mirrors the intensity on the power meter firstly decreases, but rotating the other mirror accordingly, the intensity rises to a peak greater than the original value. The beam, in the picture, has been walked in the horizontal plane to the left. The beams in figure 3.3 must be walked horizontally and vertically in order to attain maximum power at the fiber coupler FC2. Luckily, the Polaris© mirrors from ThorLabs Inc. allow precise vertical and horizontal tilting.

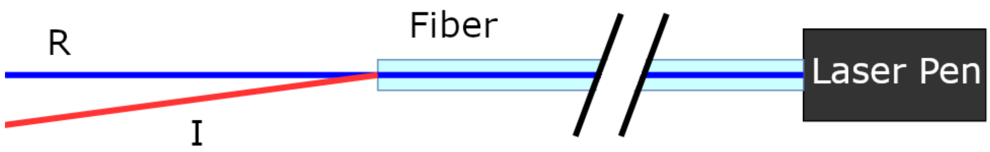

Figure A.2: The black box on the left is the laser pen, which is connected to the fiber directly. The pen generates the reference beam, which is the blue line labelled as R. The red line labelled as I is the incident laser beam from the setup, which must be tilted such that it follows the same path of the reference beam. It is important to notice that the laser pen light must have the same wavelength of the incoming beam for the eye alignment to be satisfactory; they are just presented here with different colors for the sake of clarity.

Aligning lasers into optical fibers requires a similar procedure, starting with an eye alignment and finishing with a fine, power-meter-assisted alignment. The first step consists in placing a laser pen at the other end of the fiber, as shown in figure A.2. These pens have mounts that fit into the fibers end, such that the laser from the pen is completely aligned to the fiber. The laser exits the other and at the desired angle of incidence with maximum intensity, and can be used as a reference line. By placing a paper in front of beam, and using the last aligning pair before the fiber and the techniques presented above, one must align the incident beam (red line labelled as I) such that it overlaps with the reference beam (blue line labelled as R). As soon as the eye alignment is done, the laser pen is removed and a power meter is placed at the other end. The last step consists in walking the beam with the same aligning pair such that the laser power after the fiber is maximized.

Appendix B

AOM efficiency test results

The AOM used has been tested by IntraAction prior to delivery. In this section a summary of the results obtained is presented.

Model : ATM-2001A22
IntraAction Order No. : 22229

Test Date : February 25, 2013
Test data taken by : KW

TEST CONDITIONS

Optical Wavelength : 632.8 nm
Optical Beam Diameter : 0.8 mm
RF Frequency : 200 MHz

Serial Number	RF Incident Power (Watts)	RF Reflected Power (Watts)	Diffraction Efficiency First Order (Percent)
440018	0.48	0.00	80.0

Figure B.1: Test results for the AOM used [Int13].

Appendix C

New board setup

The board has a thickness of 10 millimeters, and it is made of aluminum, as it is rigid enough to ensure no loss of alignment over time, yet it is softer and lighter than steel and thus easier to work with when drilling the holes for the screws. The setup is shown in the next page. All of the optical elements are fixed to the board with M4 screws. By defining the origin as the red cross labelled O on the lower left corner, the positions of the screw holes to be drilled are presented in table C.1. The columns x and y indicate horizontal and vertical displacement from O respectively. All of the distances, including in the setup diagram, are in millimeters. The holes have the same labelling as in figure 3.3, with three exceptions:

- Given that the AOM requires a beam height of 6.99 mm [Int13] and the beam height used is 12.446 mm, it is necessary to use an aluminum mount with two fixation points, which are the holes AOM1 and AOM2.
- As shown in figure 1.2, the beam comes from the cavity and is divided using polarizing beam splitters. The hole PBS is destined for the support of these optical devices.
- The compact setup also has a hole for a fiber coupler FC1, in case one desires to introduce light in the system using a fiber instead of the splitter. This is also helpful in the alignment process, as the splitter only diverts a portion of the beam entering into the setup, whereas the rest of the beam passes through and needs to be blocked (otherwise it becomes a stray beam). A fiber, nevertheless, exhibits less attenuation and does not generate stray beams.

Table C.1: Positions of the holes with respect to the origin O (see next page for the diagram). x indicates positive horizontal displacement to the right, y indicates positive vertical displacement upwards. All of the distances are given in millimeters.

Holes	x	y
M1A	12	79
M1B	132.5	58.5
M2A	115	300
M2B	188	301
M3A	142.5	328.5
M3B	80.5	307
M4A	39.5	53
M4B	46	112.5
PBS	51	25

Holes	x	y
AOM1	102	150.5
AOM2	164.5	150.5
L1A	104	67.5
L1B	128	262.5
L3	151.5	104
FC1	19	8.5
FC2	88	364
PD	174.5	104
I	98	104

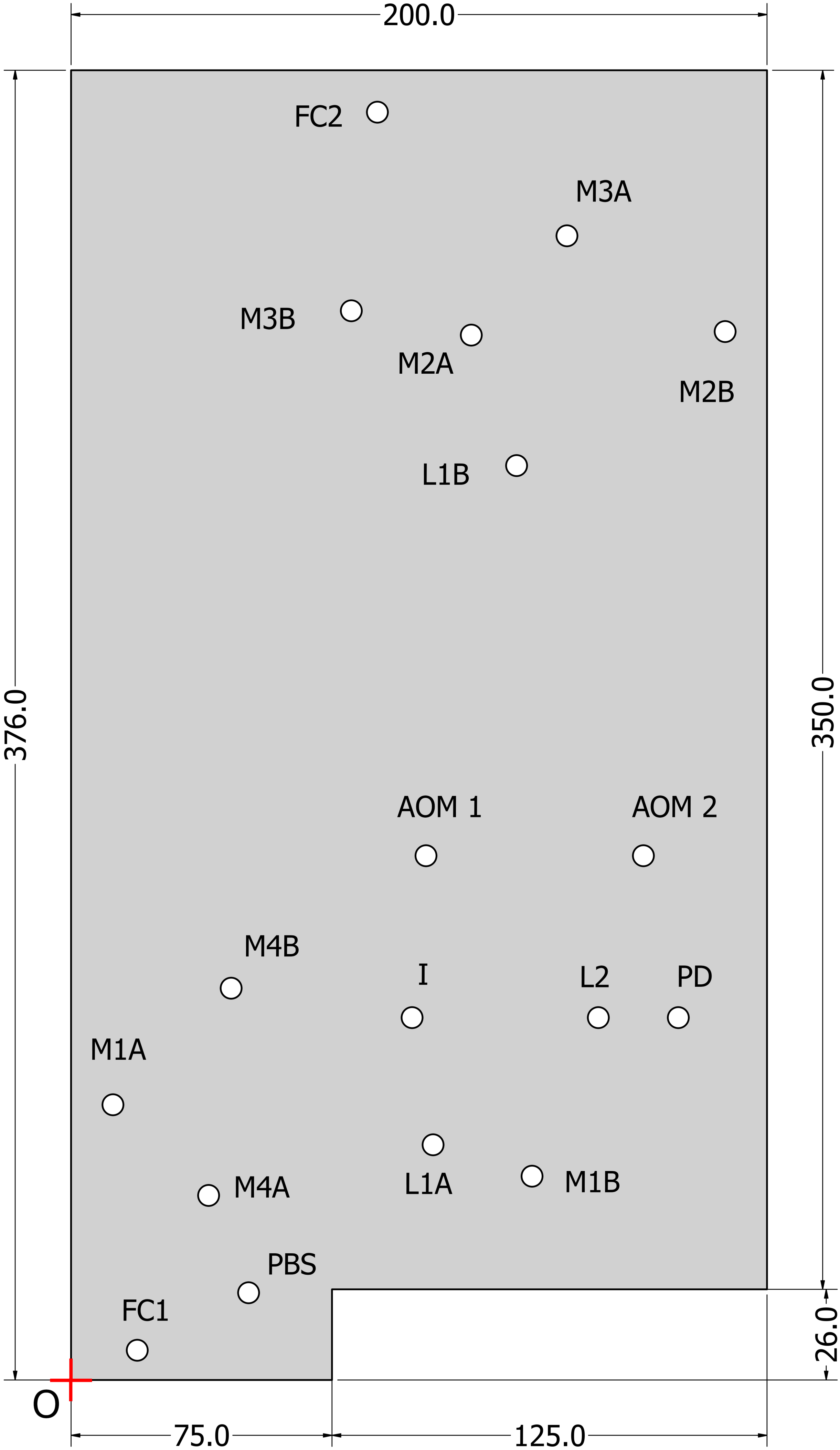
200.0
FC2
M3A
M3B
M2A
M2B
L1B
376.0
350.0
AOM 1
AOM 2
M4B
I
L2
PD
M1A
L1A
M1B
M4A
PBS
FC1
26.0
O
75.0
125.0

Bibliography

[CZ95] Juan I. Cirac and Peter Zoller, *Quantum computations with cold trapped ions*, Physical Review Letters **74** (1995), 4091–4094.

[Fis13] Karin Fisher, *Coherent control laser system for the quantum state manipulation of trapped ions*, Master's thesis, Institute for Quantum Electronics, ETH Zürich, September 2013.

[Flu14] Christa Fluehmann, *Stabilizing lasers and magnetic fields for quantum information experiments*, Master's thesis, Institute for Quantum Electronics, ETH Zürich, March 2014.

[Gab18] Matthias Gaberdiel, *Quantenmechanik I*, December 2018, Lecture Notes, Institute for Theoretical Physics, ETH Zürich.

[Hom17] Jonathan P. Home, *Physics III*, January 2017, Lecture Notes, Institute for Quantum Electronics, ETH Zürich.

[Int13] IntraAction Corporation, Belwood, IL 60104, USA, *Model ATM-2001A22 Instruction Manual*, February 2013, Serial Number 440018.

[Kie15] Daniel Kienzler, *Quantum harmonic oscillator state synthesis by reservoir engineering*, Ph.D. thesis, Institute for Quantum Electronics, ETH Zürich, May 2015.

[LYY+05] Enbang Li, Jianquan Yao, Daoyin Yu, Jiangtao Xi, and Joe Chicharo, *Optical phase shifting with acousto-optic devices*, Optics Letters **30** (2005), no. 2, 189–191.

[Mat16] Roland Matt, *Ion-trap design for magnetic-field-driven quantum information processing*, Master's thesis, Institute for Quantum Electronics, ETH Zürich, November 2016.

[Opp15] Nelson D. Oppong, *Cancelation of optical phase noise induced by an optical fiber*, Institute for Quantum Electronics, ETH Zürich, June 2015.

[Sep12] Martin A. Sepiol, *Frequency stabilization of a 729 nm diode laser to an external high finesse reference cavity*, Master's thesis, Institute for Quantum Electronics, ETH Zürich, April 2012.

[ST91] Bahaa E. A. Saleh and Malvin C. Teich, *Fundamentals of photonics*, Wiley, April 1991.

[Tho09] ThorLabs Inc., Newton, NJ 07860, USA, *LA1207-B - N-BK7 Plano-Convex Lens Specifications Sheet*, December 2009.

[Tho15] ThorLabs Inc., Newton, NJ 07860, USA, *Polaris-K05 Specifications Sheet*, December 2015.

[Tho18a] ThorLabs Inc., Newton, NJ 07860, USA, *1m, 780nm, FC/PC PM PATCH Cable Specifications Sheet*, July 2018.

[Tho18b] ThorLabs Inc., Newton, NJ 07860, USA, *1m, 780nm, FC/PC to FC APC PM PATCH Cable Specifications Sheet*, June 2018.